*Mol. Cryst. Liq. Cryst.* 1995, Vol. 266, pp. 241–262
Reprints available directly from the publisher
Photocopying permitted by license only



# CAN SPIN MODELS REPRODUCE OR PREDICT EXPERIMENTAL RESULTS IN PDLC?

CESARE CHICCOLI, PAOLO PASINI, FRANCO SEMERIA
INFN Sezione di Bologna, Via Irnerio 46, 40126 Bologna, Italy

ELISABET BERGGREN AND CLAUDIO ZANNONI
Dipartimento di Chimica Fisica ed Inorganica, Università di Bologna,
Viale Risorgimento 4, 40136 Bologna, Italy

Abstract Lattice spin models are employed to study polymer dispersed liquid crystals (PDLC). We calculate polarized light textures and Deuterium NMR lineshapes from Monte Carlo computer simulations of model nematic droplets that mimic PDLC systems with radial, toroidal and bipolar boundary conditions. We also present microscopic properties such as order parameters across the sample obtained from the simulations. Our investigations of the PDLC systems include various temperatures and external applied fields both with positive and negative susceptivity anisotropy.

## INTRODUCTION

Polymer dispersed liquid crystals (PDLC) [1] are materials that consist of nematic submicron droplets, with typical radii from a few hundred Ångström to more than a micron, embedded in a polymer matrix. These systems are interesting both for technical purposes, in view of their applications in optical devices [2], but also for studying the behavior of mesophases in a confined environment [3,4]. Moreover PDLC droplets represent practical examples of systems exhibiting topological defects that are of interest in many fields of physics [5]. The properties of the nematic/polymer interface depend on the characteristics of the polymer matrix and the preparation methods, which give rise to different boundary conditions at the droplet surface, for example radial [3,6,7], axial [6,7], toroidal [8,9] and bipolar [3,7,10] ones. The molecular organization inside the droplet results from the competition between the effects due to the surface boundary condition, those of molecules trying to arrange themselves parallel to each other in the nematic phase and the disordering of the phase due to temperature. Other effects of interest are caused by the application of an external, electric or magnetic, field [3]. The first studies on these systems have been carried out experimentally by X-ray, neutron scattering and electron microscopy [11]. Later PDLC have mainly been investigated using deu-

terium NMR [3] and polarized light microscopy [7,12] for droplets below and above micron size, respectively.

Theoretically PDLC have been studied using continuum elastic theories [6,7,13,14] originally developed for bulk systems. More recently we have studied PDLC using Monte Carlo simulations in a variety of physical situations: different boundary conditions [15,16,17], influence of the anchoring strength at the nematic/polymer interface [16,18] and the effect of an external applied field [17,19,20]. We have tried to render computer simulations practically useful by calculating quantities that can be directly observed attempting to cover, in this way, the gap with experimental investigations performed on the same systems. We have developed methodologies to calculate powder deuterium NMR lineshapes [17,19] and textures observable in polarized light experiments [20] corresponding to the microscopic configurations found. Here we wish to present simulation results for a number of relevant cases including three different boundary conditions: radial, toroidal and bipolar. We investigate the orientational order and the molecular organization in these systems for various anchoring strengths and for external applied fields of different magnitude both for positive and negative susceptivity anisotropy [12]. Field effects have also been studied experimentally [3,12], and it is possible to compare the simulation results with these at least in some cases. We also study the effect that the application of a field has on the ordering inside the droplet and the modifications that the field induces on the phase transition behavior and molecular organization. For all cases treated the calculations are performed at various temperatures.

## PDLC LATTICE SPIN MODELS

### The Model System

Monte Carlo simulations of lattice spin models have been used in studying liquid crystals since the pioneering work of Lebwohl and Lasher (LL) [21]. The restriction of considering the molecules with fixed positions at the lattice sites does not alter in any essential way the long range orientational behavior. The LL model reproduces well the characteristics of a weakly first order nematic-isotropic phase transition as observed in real nematics [22], and moreover lattice models present various advantages for the study of collective properties in comparison with more "realistic potentials" which also includes traslational degrees of freedom such as, for example, the Gay-Berne model [23]. The main advantage of lattice models is connected with their simplicity, which makes it possible to treat a relatively large number of particles, or "spins". We recall that, up to now, the largest Gay-Berne simulation has been performed on systems of about a thousand molecules while calculations on LL samples thirty times larger have been presented by several groups [22,24,25]. As an alternative, using smaller lattices gives the possibility of investigating potentials for more complicated systems depending on additional parameters, for example boundary conditions and field strengths, over a wide grid of temperatures, as is the case for the nematic microdroplets. In the model system each spin represents a closely packed group of molecules that maintains its short range order across the nematic/isotropic phase transition [26] or, as a special case,

a single molecule. In other words in this coarse grained interpretation the model really describes the order-disorder of short range ordered clusters of molecules, and typically one of these microdomains could consist of up to $10^2$ particles.

The PDLC model consists of an approximately spherical sample $\mathcal{S}$ carved from a cubic lattice with spins interacting with the LL potential [15–18] while the surface effects are modelled with a layer of outside "ghost" spins, $\mathcal{G}$, with orientations mimicking the desired boundary conditions. Each spin is represented by a unit vector $\mathbf{u}_i$ and the pair interaction is then assumed to be:

$$U_{i,j} = \begin{cases} -\epsilon_{ij}\left[\frac{3}{2}(\mathbf{u}_i \cdot \mathbf{u}_j)^2 - \frac{1}{2}\right], & \text{for } i,j \in \mathcal{S} \\ -\epsilon_{ij} J\left[\frac{3}{2}(\mathbf{u}_i \cdot \mathbf{u}_j)^2 - \frac{1}{2}\right], & \text{for } i \in S, j \in \mathcal{G} \end{cases} \tag{1}$$

where $\epsilon_{ij}$ is a positive constant for the spins $i$ and $j$ if they are nearest neighbors and zero otherwise. The parameter $J$ accounts for the effect of different anchoring strengths to the polymer surface. When the interaction between two neighbors, one on the surface of the nematic droplet and one belonging to the outside matrix, is the same as that between two liquid crystal spins then $J = 1$, while $J = 0$ would correspond to a droplet in vacuum. We have investigated the following three different boundary conditions at the interface nematic/polymer:

*i)* Radial boundary conditions, (RBC) are mimicked by letting the spins in the matrix be oriented normally to the local surface, so that they point towards the center of the droplet.

*ii)* Toroidal boundary conditions, (TBC) are obtained when the spins in the polymer interface lie in planes perpendicular to the $z$ axis and are orientated tangentially to the droplet surface.

*iii)* Bipolar boundary conditions, (BBC) for which the ghost spins are oriented tangential to the droplet surface and in planes parallel to the $z$ axis.

Our Monte Carlo methodology, using a standard Metropolis procedure [22] to update the lattice, is described in details in our previous papers [15–18]. Here we only mention that during the present PDLC studies we have performed a number of simulations for system sizes ranging from 304 to 11752 spins over a wide range of temperatures (about 40). Several thermodynamic observables have been calculated: energy $U$, dimensionless heat capacity $C_V^*$, overall second and fourth rank order parameters, $\langle P_2 \rangle_\lambda$ and $\langle P_4 \rangle_\lambda$, obtained from eigenvalues of the ordering matrix [22], and radial [15,18], toroidal[16] and bipolar [20] order parameters that we have introduced to quantify the deviations from a perfect radial, toroidal and bipolar configuration, respectively.

The application of an external electric or magnetic field can be modelled by adding another second rank term to keep into account the coupling. Thus inside the sphere we have the $N$ particle hamiltonian:

$$U_N = -\sum_{\substack{i,j \\ i<j}} \epsilon_{ij}\left[\frac{3}{2}(\mathbf{u}_i \cdot \mathbf{u}_j)^2 - \frac{1}{2}\right] - \epsilon\xi \sum_{i=1}^{N}\left[\frac{3}{2}(\mathbf{u}_i \cdot \mathbf{B})^2 - \frac{1}{2}\right] \tag{2}$$

where B is a unit vector along the field direction that we take to define the laboratory $z$ axis and $\xi$ determines the strength of the coupling to the field. This kind of potential has been used some years ago to investigate the application of an external field on a nematic bulk system [27], and recently we have studied this model in the cases of nematic droplets with radial and bipolar boundary conditions [17,19,20]. The parameter $\xi$ depends on the appropriate susceptivity anisotropy and field strength as we have discussed elsewhere [19].

Simulation Results

As already mentioned, the LL model shows a first order phase transition for the bulk, while in a confined system, of sufficiently small size and with fixed boundary conditions, the phase transition is suppressed [18]. This was experimentally observed by Crawford and Doane [1] and was clearly shown by Iannacchione et al [28] in the experimental behavior of the heat capacity for 5CB confined in anopore membranes. The maximum of the heat capacity curves at the nematic/isotropic transition is generally smaller for the nematic confined both with radial and axial boundary conditions in comparison with the bulk.

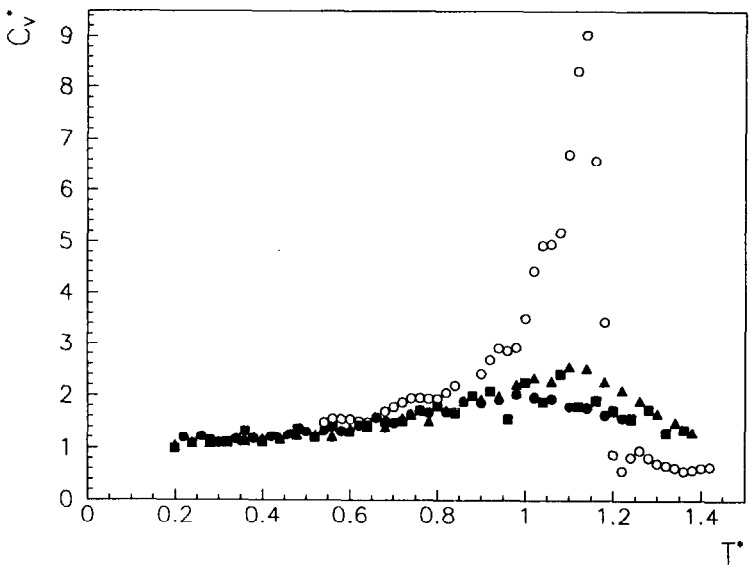


FIGURE 1. Specific heat per particle (dimensionless units), $C_V^*$, versus temperature for a model nematic droplet with 304 particles and radial (●), toroidal (■) and bipolar (▲) boundary conditions. Results of a simulation performed on the same system size with cluster boundary conditions [29] mimicking a bulk sample (○) are also presented.

This behavior is at least qualitatively reproduced by lattice models as shown in Figure 1 where the results from calculations on systems containing 304 spins are presented both for the bulk and for nematic droplets with radial, toroidal and bipolar boundary conditions. Although no major modifications appear in the heat capacity behavior, the various boundary conditions produce a great difference in the molecular organization, as can be observed from the Monte Carlo configurations shown in Figure 2. The "snapshots", presented as a horizontal and a vertical cross section through the center of a simulated droplet for each of the three boundary conditions here discussed, are taken from MC simulations including 5832 spins at $T^* = 0.4$.

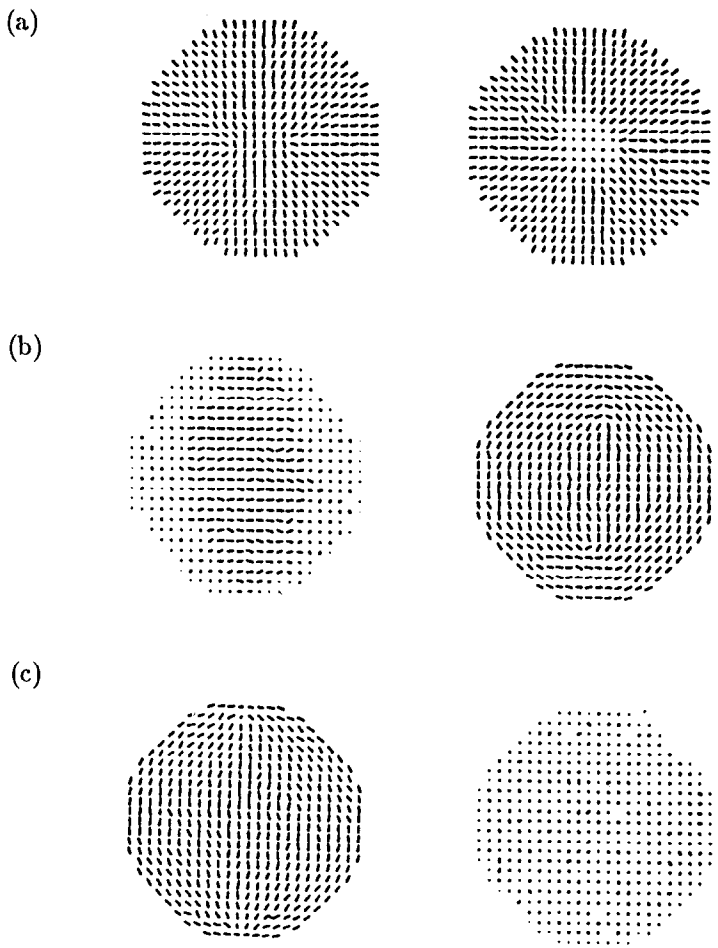


FIGURE 2. "Snapshots" of droplet configurations for three different boundary conditions, radial (a), toroidal (b) and bipolar (c). We show, on the left, a vertical cross section ($xz$ plane) and, on the rigth, a horizontal section ($xy$ plane) for each case.

The differences between the three cases are also apparent looking at the standard second order parameter $\langle P_2 \rangle_\lambda$, obtained from the diagonalization of the ordering matrix [22], which quantifies the overall nematic order of the system. The temperature dependence of $\langle P_2 \rangle_\lambda$ for the three different boundary conditions is presented in Figure 3. For the radial case we find a complete absence of nematic order when the interaction with the surface is of the same strength as between the particles inside the droplet, i.e. $J = 1.0$ (see Figure 3a). At low temperature only a small core at the center [18] shows alignment of particles but this is not sufficient to outbalance the radial ordering induced by the surface. Increasing the temperature the size of the core tends to increase but at the same time the nematic order inside this region decreases and then $\langle P_2 \rangle_\lambda$, which is an average over all the spins of the droplets, becomes even smaller. The nematic ordering becomes favoured as the planar surface alignement increases as for the toroidal and, to an even greater extent, for the bipolar boundary conditions. So, as expected, for $J = 1$ the bipolar case is characterized by a greater nematic order in comparison with the radial and toroidal configurations as clearly shown in Figure 3a. Decreasing the strength of the anchoring $J$, the alignment induced by the surface becomes weaker and for, an interaction with the ghost particles equal to one fourth of that inside the droplet ($J = 0.25$), the three cases show very similar curves for the nematic order parameter $\langle P_2 \rangle_\lambda$ (Figure 3c).

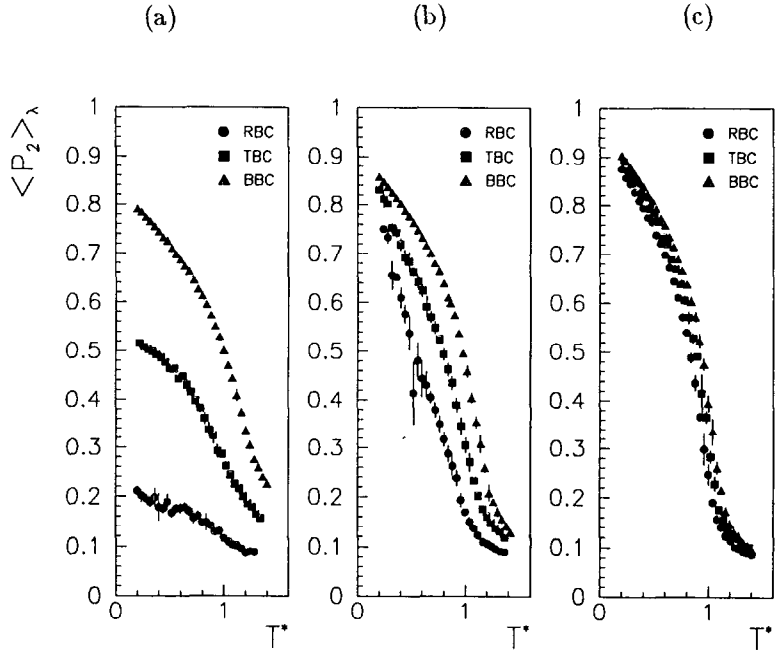


FIGURE 3. The order parameter $\langle P_2 \rangle_\lambda$ plotted against temperature for radial (RBC), toroidal (TBC) and bipolar (BBC) boundary conditions for different values of the anchoring strength parameter $J$. Results for $J = 1$ (a), $J = 0.5$ (b) and $J = 0.25$ (c) are shown.

One of the advantages of simulations is the possibility of calculating a variety of microscopic observables. For a better understanding of the ordering inside the droplet we have also calculated the second order parameter, $\langle P_2 \rangle_\lambda$ across the droplet, in concentric regions (shells) dividing the spherical sample in an onion like way[18]. So that we have four, seven, eleven and fourteen shells for droplets including 304, 1476, 5832 and 11752 spins, respectively. In Figure 4 the resulting order parameters are plotted as a function of the distance from the droplet center in lattice units for the three different boundary conditions here discussed. We have also plotted $\langle P_2 \rangle_\lambda$ against a relative distance defined as $r/r_{max}$, where $r_{max}$ is the radius of the sphere, to investigate if the ordering inside the droplet depends on the system size or if the behavior is just the same in these reduced units as in lattice units. As mentioned earlier we expect, for the radial case, the nematic order to be greater near the core of the droplet (inner shell) and to decrease in the other shells. It is interesting to notice that in this case the size of the aligned core does not depend on the droplet size and has a radius of about 3-4 lattice units [30] (see Figure 4a) for all the system sizes studied. This hints that the core size is a true material property [30] rather than being dependent on the droplet size. The picture changes completely when going to a planar surface achoring: the nematic ordering at the surface becomes larger for the toroidal boundary conditions and then even larger for the bipolar case with respect to the radial one (Figures 4b-c). Moreover the aligned region at the center becomes larger and, above all, its size increases linearly with the droplet radius yielding almost superimposed curves for the different system sizes, as shown on the right in Figures 4b-c. We can then say that the size effect is neglible from this point of view, although different results are achieved for the homeotropic (radial) and planar (toroidal and bipolar) surface alignment.

As far as the effect of an external field is concerned, we present the simulation of a nematic droplet with radial boundary conditions. We have performed calculations at various system sizes with fields of different intensities and with both positive and negative susceptivity anisotropy. Here we report results for $\xi = -0.05, -0.20, -0.50, 0.05, 0.20$ and $0.50$. From a thermodynamic point of view the main effect of the external field is a slight shift of the heat capacity peak towards a higher temperature, in accord with the stabilization of the ordering induced by the applied field[19]. We have calculated the nematic, $\langle P_2 \rangle_\lambda$, the radial $\langle P_2 \rangle_R$, and field $\langle P_2 \rangle_B$, order parameters, and in Figure 5 we present a summary of the results for these order parameters versus temperature. The applied field produces an alignment of the spins inside the droplet, with a consequent enhancement of $\langle P_2 \rangle_\lambda$, when the anisotropic coupling is positive. In fact in this case the molecules tend to align along the field direction (here the $z$ axis), while, of course, for negative coupling they tend to align normally to the field and to lie in the $xy$ plane. The effect is also evident when looking at the radial order parameter $\langle P_2 \rangle_R$ which presents a standard "decrease with temperature" behavior also for the higher negative field coupling. This is because the molecular organization inside the droplet is consistent with a set of discs (perpendicular to the $z$ axis) on which the spins, especially at low temperatures, are radially oriented. A further confirmation of the alignment of the spins normally to the $z$ axis is given by the

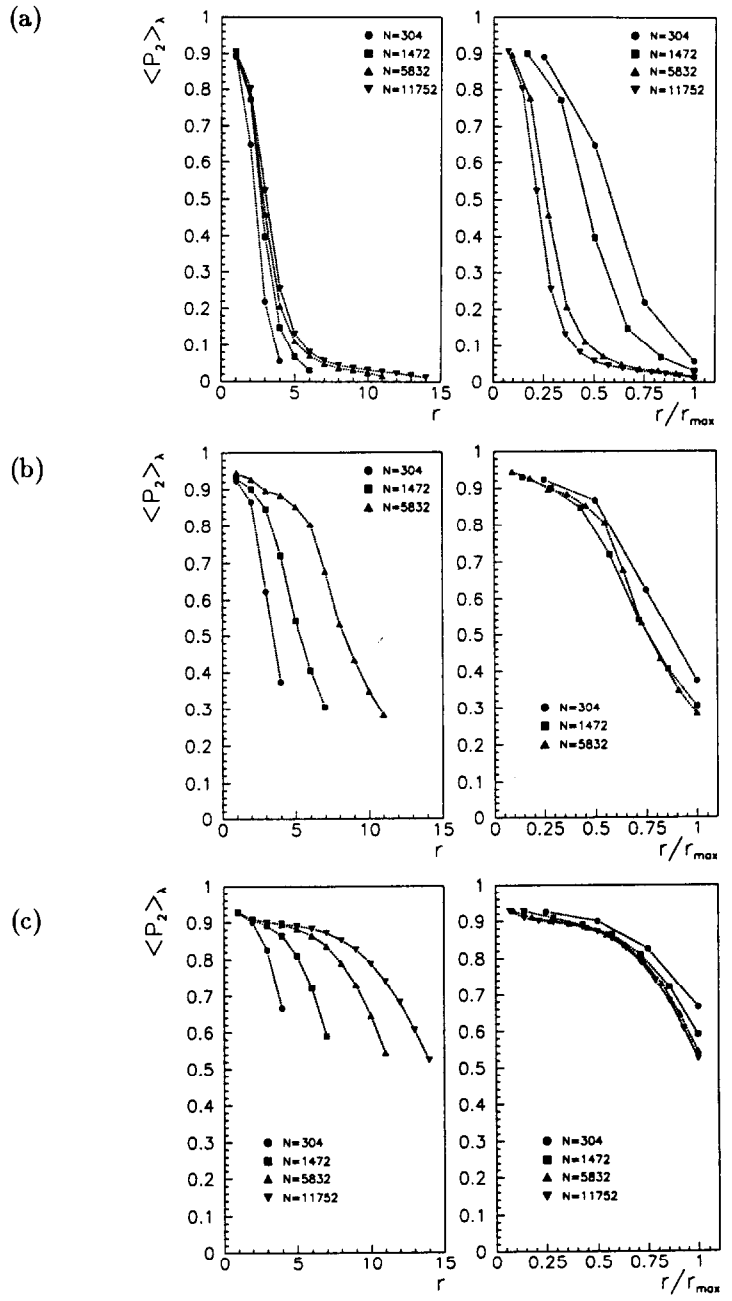


FIGURE 4. The order parameter $\langle P_2 \rangle_\lambda$ studied versus distance from the droplet center, $r$, in lattice units (left) for radial (a), toroidal (b) and bipolar (c) boundary conditions at the reduced temperature $T^* = 0.4$. For each case, in the plates on the right, $\langle P_2 \rangle_\lambda$ is plotted against the normalized radius, $r/r_{max}$.

calculations of the field order parameter $\langle P_2 \rangle_B$ shown in Figure 5c. The results for the negative coupling are approximatively one half of those for the corresponding positive field strength.

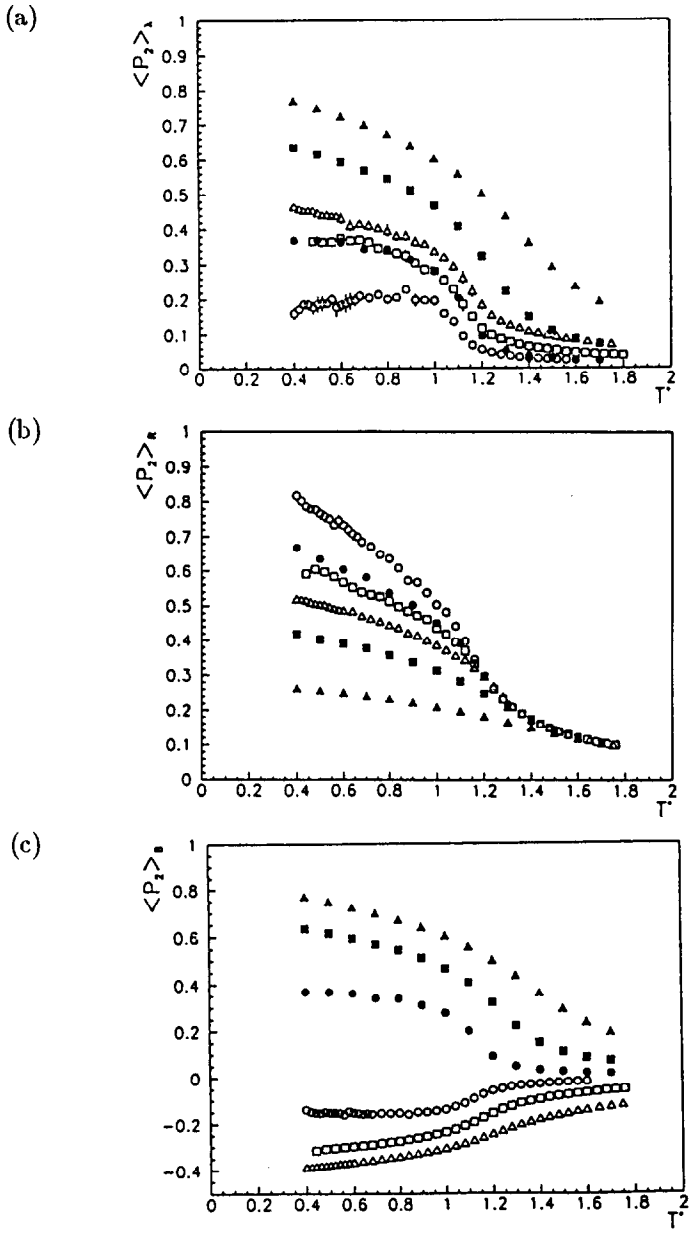


FIGURE 5. The nematic, $\langle P_2 \rangle_\lambda$ (a), radial $\langle P_2 \rangle_R$ (b) and field $\langle P_2 \rangle_B$ (c) order parameters against reduced temperature for negative and positive coupling and different field strengths: $\xi = -0.05$ (○), $-0.20$ (▫), $-0.50$ (△), 0.05 (●), 0.20 (■) and 0.50 (▲).

## FROM SIMULATION RESULTS TO EXPERIMENTAL OBSERVABLES

### Deuterium NMR Lineshapes

Deuterium NMR of deuterated liquid crystals is probably the experimental technique most often used in studies of sub-micron PDLC droplets [3,10], because of the possibility to deuterate only the molecules inside the droplet while the molecules in the polymer matrix remain undeuterated. This allows a direct observation of the molecules inside the droplet. The actual spectrum obtained will depend on the time scale of the dynamics of spins changing from one ordered domain to another. In the limit of very fast motion an average, single line, spectrum would be expected, with a somehow limited information on the underlying molecular organization. The opposite limit, of frozen domain motion on the experimental time scale is more interesting. We have calculated deuterium NMR lineshapes in the limit of no relevant dynamics as a powder spectra[17,19,20], from the average of a number (here 20) instantaneous simulated configurations to improve signal to noise ratio. Each configuration is given as a set of direction cosines of fictitious uniaxial domains with the angle $\beta_j$ between the spin axis and the $z$ axis defined for the droplet (in case of an external field, this is applied along the $z$ axis). Each of these domains contributes to the powder lineshape, $\mathcal{S}(\omega)$, with a doublet type of spectra, given by:

$$\mathcal{S}(\omega, \omega_Q(\cos\beta_j), T_2^{-1}) = \sum_{m=\pm 1} \frac{T_2^{-1}}{(\omega + m\omega_Q(\cos\beta_j))^2 + (T_2^{-1})^2} \tag{3}$$

where the two transition frequencies are at $\omega_Q(\cos\beta_j) = \pm\nu_Q P_2(\cos\beta_j)P_2(\cos\theta)$, and $\nu_Q$ is the quadrupole coupling constant and $\theta$ is the angle between the effective quadrupole axis and the molecular axis. The intrinsic linewidth, $T_2^{-1}$, is set to 200 Hz in the calculations. The sample average giving the total spectrum originating from one configuration is then calculated as

$$\begin{aligned} \mathcal{S}(\omega) &= \langle \mathcal{S}(\omega, \omega_Q(\cos\beta_j), T_2^{-1}) \rangle_S \\ &= \frac{1}{N} \sum_{i=1}^{N} \mathcal{S}(\omega, \omega_Q(\cos\beta_j), T_2^{-1}). \end{aligned} \tag{4}$$

where $N$ is the number of particles in the configuration. The parameters that we have used here are appropriate to $4' - methoxy - 4 - cyanobiphenyl - d_3$ (10CB) [3,17,19,20]. The results are presented for the three cases of boundary conditions in the following subsections.

We have already shown that Deuterium NMR lineshapes for different droplet sizes ($N = 11752$ and $N = 5832$) [20] are superimposable. This indicates that our results could be applied also to larger droplets, and confirms that it is appropriate

to consider that one spin is a representative of a group of molecules [26] rather than a single molecule. Following this discussion it is maybe not too far fetched to assume that the present results are applicable even if the droplets are of micron size so that it is possible to investigate them using polarized light microscopy (sizes of at least $2-3\mu m$ are needed [7]). This would then require a scaling factor of the order of $10^2$ for low molar mass nematic droplets. To test that this gives reasonable results we have earlier calculated the optical textures for different droplet sizes ($N = 304, 5832$ and $11752$) [20], obtaining no qualitatively change from one size to another but only an improvement of the resolution with a larger amount of sites inside the sample. We have therefore found it of interest to calculate the optical textures for the RBC, TBC and BBC cases for different fields and temperatures, which we present in the following subsections together with the Deuterium NMR lineshapes to give a more complete prediction of these observables for PDLC.

Polarized Light Textures

The calculation of a polarized light texture is performed using a standard matrix approach which has been employed in calculations based on continuum theory [7,12,32] as well as in our MC work on BBC droplets [20]. The basic idea in the matrix approach is that ray optics can be used and that each site in the droplet is described by a Müller matrix[31]. Then the light ray passing through a row of particles across the droplet is retarded by the matrix resulting from the product of the Müller matrices corresponding to each particle in the light path. In this matrix are involved the angles $\phi_j$ and $\theta_j$, describing the position of a domain $j$, taken from the simulation data, and the phase difference which depends on the thickness of the layer, $h$, the wave length, $\lambda$, and the refractive indices, $n_0$ and $n_e$. We have used $h = 5.3\mu m/(2r_{max})$ ($r_{max}$ is the radius of the droplet in lattice units), $\lambda = 545nm$, $n_0 = 1.5$ and $n_e = 1.7$, that should be similar to those of the nematic liquid crystal 5CB [7]. Since we assume the local domain to be basically unchanged throughout the simulations, that only describe the disordering of a domain with respect to the others, we have arbitrarily taken this intrinsic refractivity to be constant with temperature.

To observe the light retarded by the droplet we assume to have crossed polarizers placed at each side of the sample, $\mathrm{P}_{in}$ and $\mathrm{P}_{out}$, and the resulting Stokes vector of the polarized and retarded light beam is thus given by [12,31]

$$\mathbf{s} = \mathrm{P}_{out} \prod_j \mathrm{M}_j \mathrm{P}_{in} \mathbf{s}_{in} \tag{5}$$

where $\mathbf{s}_{in}$ corresponds to the Stokes vector of unpolarized light. The intensity is proportional to the first element in the output Stokes vector $\mathbf{s}$. To improve the quality of the optical image we have, as in the NMR lineshape calculations, averaged over a sufficiently large number of equilibrated configurations. The results presented here are obtained from averages over 20 configurations sampled every 2000 cycles.

A texture obtained from configurations defined by a lattice of $22 \times 22 \times 22$, corresponding to a droplet of 5832 particles, is a projection of $22 \times 22$ pixels perpendicular to the direction of the retarded and polarized lightbeams. The intensity of each pixel is grey coded for each picture with a normalized scale going from black, lowest intensity of light, to white, highest intensity, with 32 different grey levels.

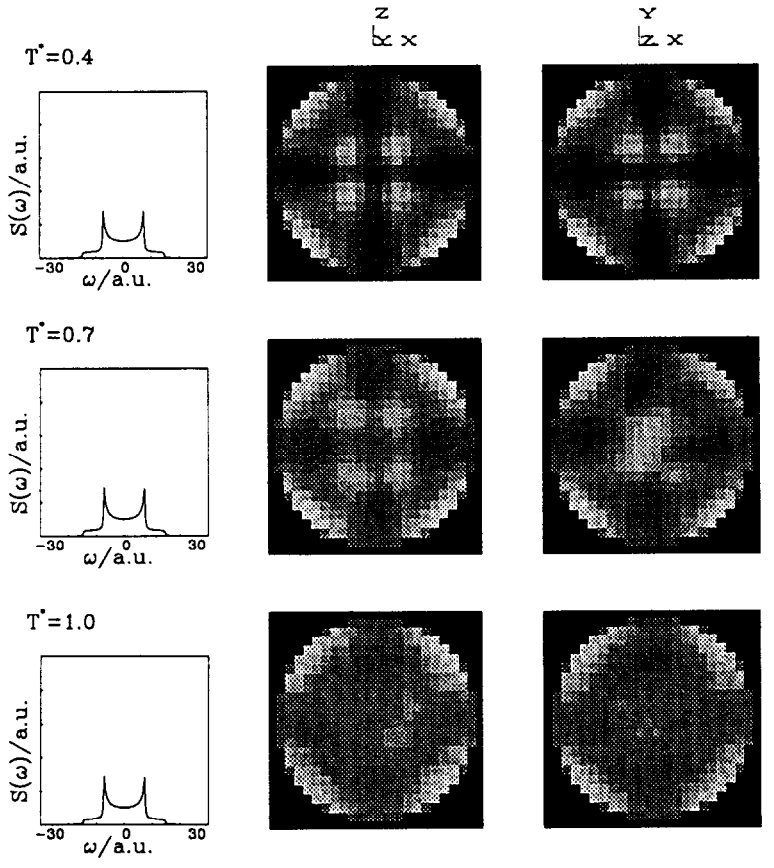


FIGURE 6. Deuterium NMR lineshapes (left) and polarized light textures projected with the light propagation direction coinciding with the $y$ axis (middle) and the $z$ axis (right) at three temperatures, $T^* = 0.4$ (top), 0.7 (middle) and 1.0 (bottom). The boundary conditions are radial, and there is no applied field.

## RESULTS OF CALCULATED OBSERVABLES

### Radial Boundary Conditions

If we first consider the case of no applied field at low temperature, the boundary condition, assuming strong anchoring ($J = 1.0$), is determining the ordering inside the droplet, so that almost all sites are radially oriented with a correspondent radial order parameter, $\langle P_2 \rangle_R$ close to 1 [19]. This "star" organization gives an isotropic powder spectra, shown in Figure 6, at $T^* = 0.4$. For the higher temperatures the lineshape remains unchanged, even if the actual configuration inside the droplet is changing from a radially ordered one (see Figure 5) to a truly isotropic phase, which cannot be distinguished from the NMR lineshape. The first observation to be done in studying the polarized light textures in Figure 6 is that the two projections, with the light propagation

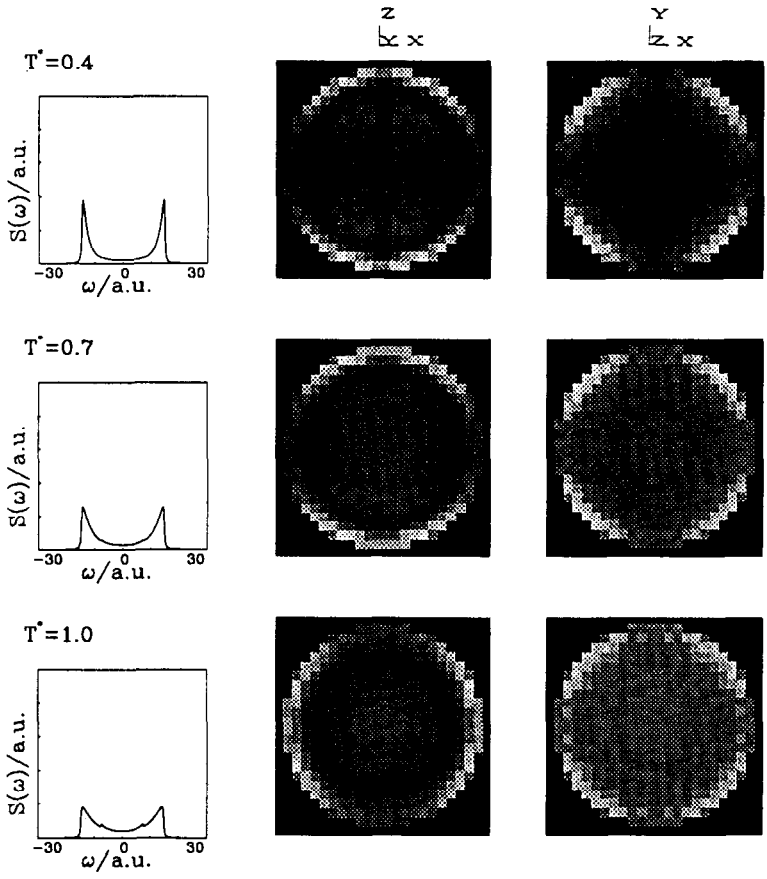


FIGURE 7. Same as Figure 6 for a positive applied field, $\xi = 0.5$.

coinciding with the $y$ and $z$ axes, respectively, are essentially the same. At low temperature the dark cross indicates the spins aligned with either of the crossed polarizers for the radial configuration. At higher temperature the dark cross disappears as the domains become disordered. We have then got some information about the internal ordering of the droplet from the polarized light textures that was not appearent from the correspondent Deuterium NMR lineshape. It should be said of course that we have assumed static spectra to be observable at the different temperatures. In a real situation the extent of spin diffusion will increase with temperature and a single isotropic line could then be observed.

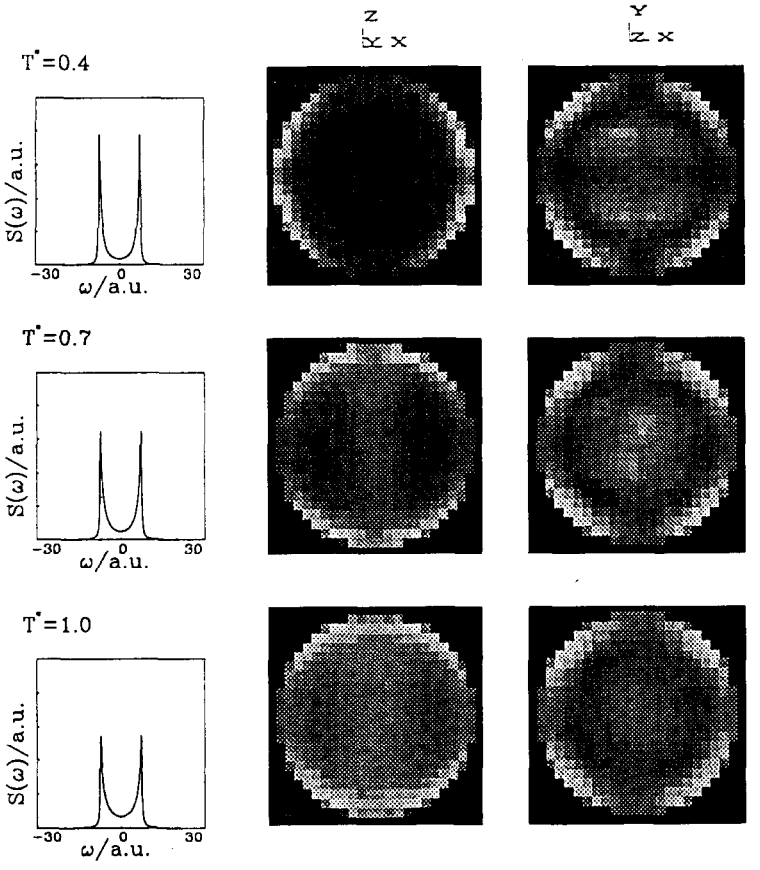


FIGURE 8. Same as Figure 6 for a negative applied field, $\xi = -0.5$.

We now apply a field along the $z$ axis of the system. The resulting lineshapes

and optical textures for a positive susceptivity anisotropy, $\xi = 0.5$ are presented in Figure 7. At low temperature a majority of the sites inside the droplet are directed along the field and the quadrupole splitting in the NMR spectra essentially corresponds to $\beta_j = 0$ (Eq. 3), and $P_2(\cos 0) = 1$. Qualitatively the same results were obtained experimentally by Golemme et al [3]. The applied field produces a difference in the two projections of the optical textures. It is possible to observe that the domains are parallel or perpendicular to the $z$ axis (dark areas in textures) and that the radial ordering is present only close to the surface.

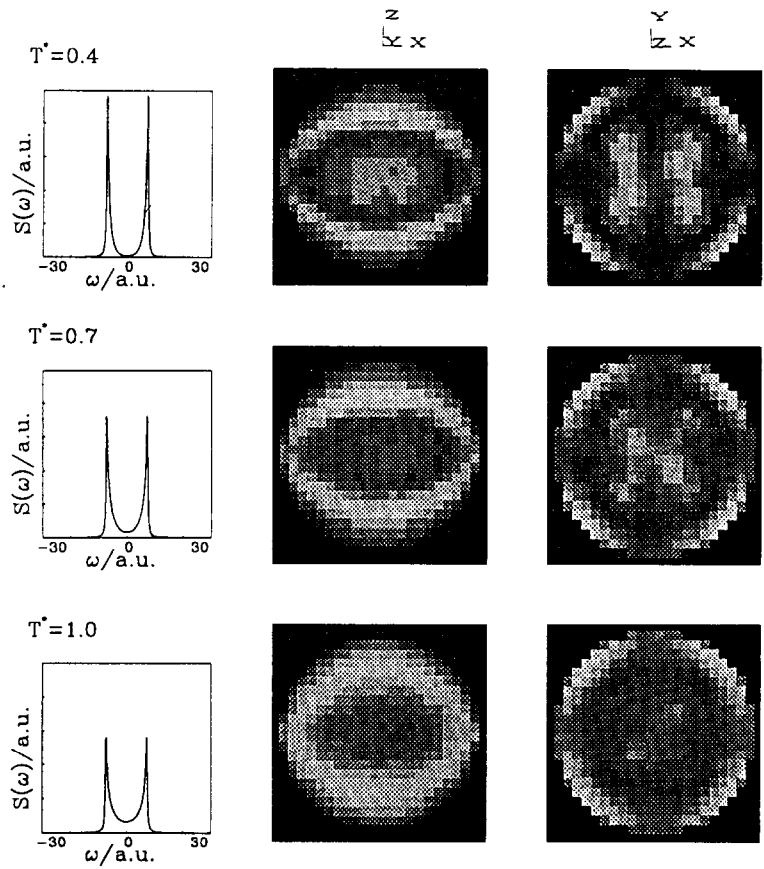


FIGURE 9. Deuterium NMR lineshapes (left) and polarized light textures projected with the light propagation direction coinciding with the $y$ axis (middle) and the $z$ axis (right) at three temperatures, $T^* = 0.4$ (top), 0.7 (middle) and 1.0 (bottom). The boundary conditions are toroidal, and there is no applied field.

The results from application of an external field in the case of a negative susceptivity anisotropy, $\xi = -0.5$, are presented for different temperatures in Figure 8. The anisotropy of a negative field favours an orientation of the particles perpendicular to the field direction [12] (the $z$ axis) rather than alignment parallel to the field, as for the case of positive susceptivity. From the NMR lineshape we observe that most spins are oriented perpendicular to the $z$ axis, $P_2(\cos(\pi/2)) = -1/2$, i.e. the quadrupole splitting is half as big as observed for $\xi = 0.5$ (Figure 7). Concerning the optical textures we see in the projection perpendicular to the $z$ axis that a dark cross is visible, which is consistent with the "star" pattern being conserved in the $xy$ planes. In the lineshape and especially in the textures we observe some disordering due to the increasing temperature.

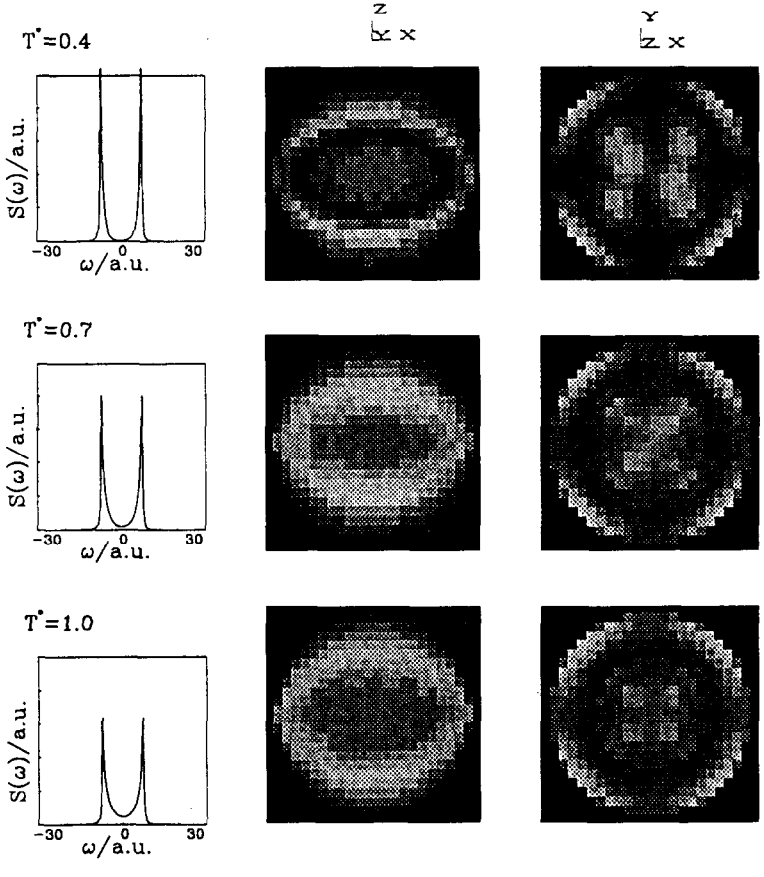


FIGURE 10. Same as Figure 9 for a negative applied field, $\xi = -0.5$.

Toroidal Boundary Conditions

We first show results for a simulated toroidal droplet in the absence of an applied field (Figure 9). From the transition frequencies in the NMR spectra we observe that most of the spins are oriented perpendicularly to the $z$ axis consistently with the boundary conditions. In the optical textures perpendicular to the $z$ axis (right) we see a symmetric pattern corresponding to a symmetric distribution of the spins around the axis of the toroidal boundary structure. In the other projection the spins ordered in planes perpendicular to $z$ appear in the texture as a dark almond shaped core.

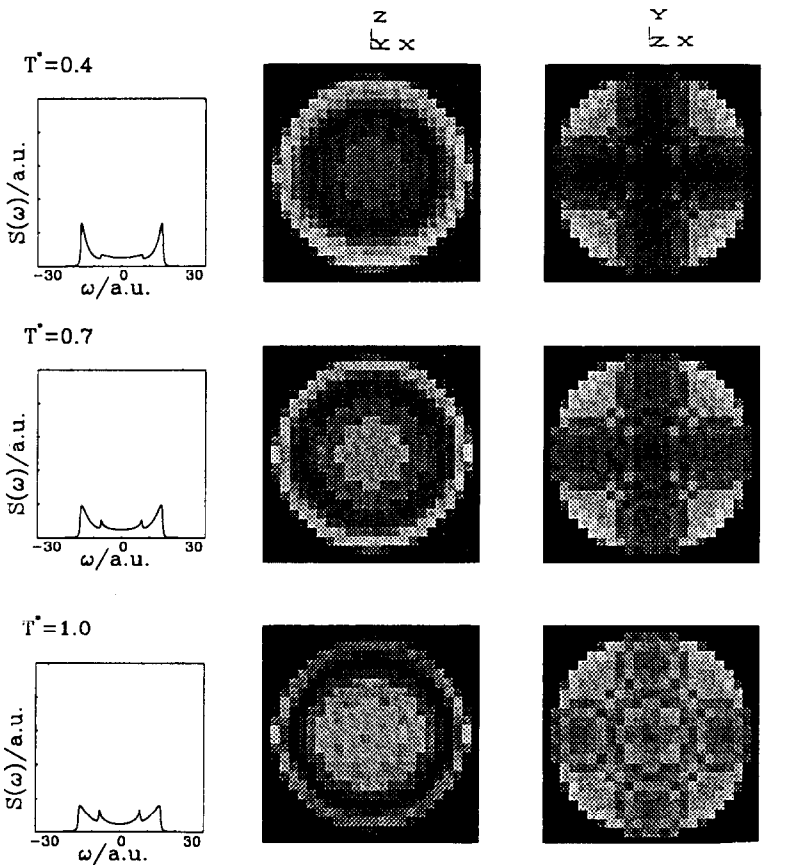


FIGURE 11. Same as Figure 9 for a positive applied field, $\xi = 0.5$.

If a negative field is applied to the sample, the characteristics already observed for the case with $\xi = 0$ become more pronounced for the NMR-lineshape as well as for the polarized light textures (Figure 10), because the negative susceptivity

anisotropy has the effect of trying to align the molecules perpendicular to the field direction which, we recall, is along the toroidal boundary conditions axis. More interesting is perhaps to observe the predictions for a positive field that opposes the effect of the toroidal boundary condition (Figure 11). At low temperature the population of sites parallel to the applied field is bigger than that perpendicularly ordered. In the texture projected perpendicular to the field the dark core has disappeared. The star pattern is always observed in the $xy$ projection, and is more distinguishable than for $\xi = 0$ or $-0.5$.

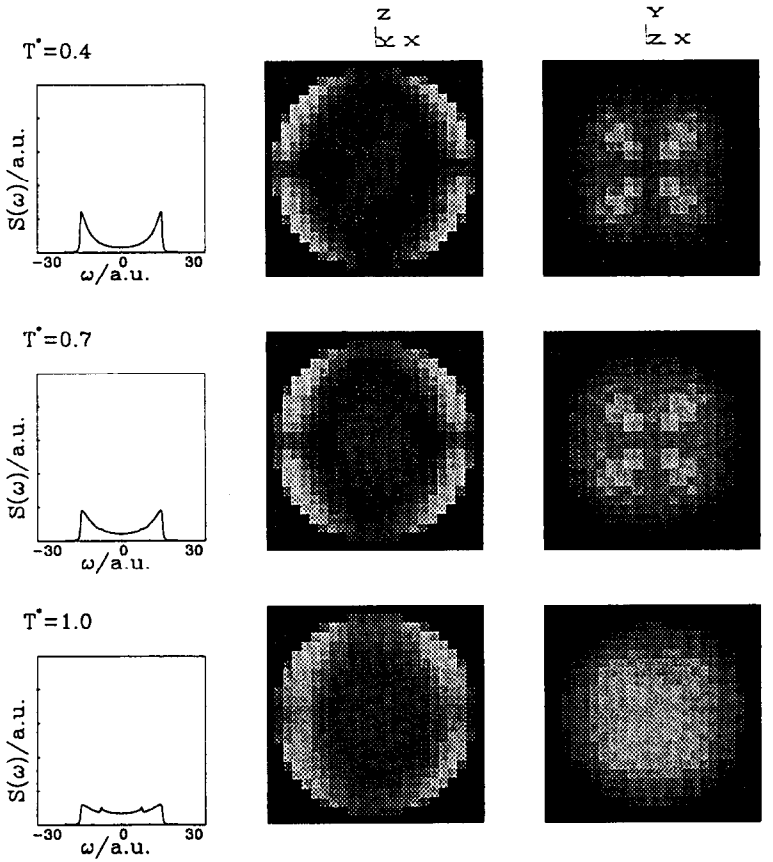


FIGURE 12. Deuterium NMR lineshapes (left) and polarized light textures projected with the light propagation direction coinciding with the $y$ axis (middle) and the $z$ axis (right) at three temperatures, $T^* = 0.4$ (top), 0.7 (middle) and 1.0 (bottom). The boundary conditions are bipolar, and there is no applied field.

Bipolar Boundary Conditions

We have already described this case elsewhere [20] and here we review the Deuterium NMR lineshapes and the polarized light textures obtained to compare them with the results of the other boundary conditions presented. In Figure 12 we show the observables when no external field is present. The NMR linehape at low temperature confirms that the bipolar boundary conditions induce a larger nematic order with a preferred direction parallel to the $z$ axis [3,10], i.e. they have an orientation perpendicular to the one of the corresponding case for the toroidal droplet (Figure 9), while the radial droplet is giving an isotropic powder spectrum (Figure 6) under the same circumstances.

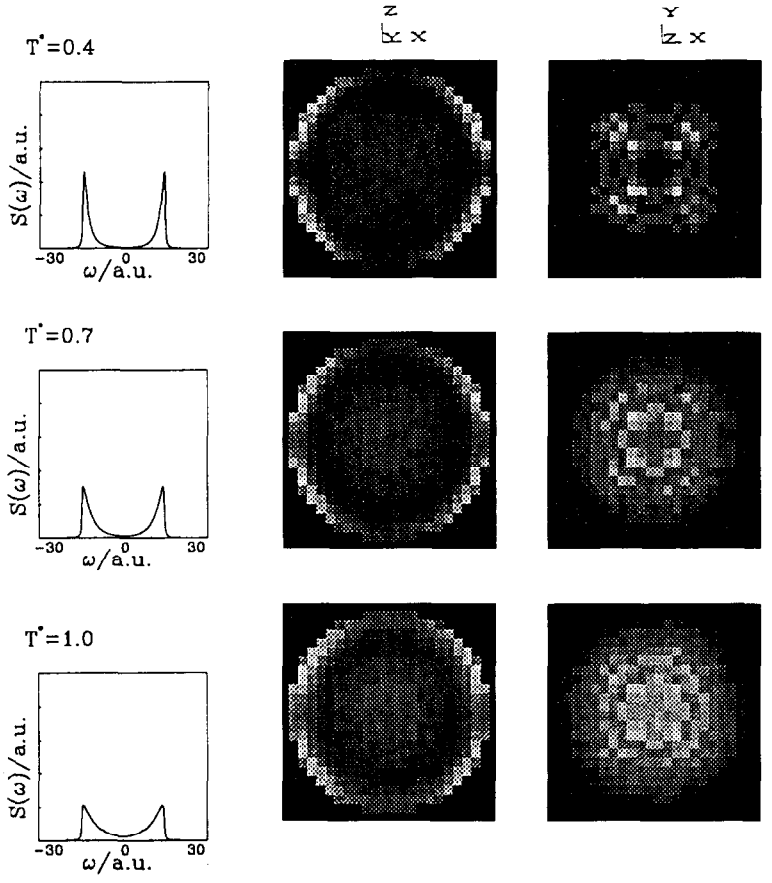


FIGURE 13. Same as Figure 12 for a positive applied field, $\xi = 0.5$.

The texture resulting from light propagating in the $y$ direction shows that in the core of the droplet all the spins are parallel ordered, while the $xy$ projection shows

that the spins are forming a "star" pattern in the planes parallel to the $z$ axis. The simulated textures are qualitatively in agreement with those experimentally observed by Ondris-Crawford et al [7]. The results of application of an external field with positive susceptivity are presented in Figure 13, where the spins are forced to be directed parallel to the field.

The textures and lineshapes from application of a field when the susceptivity anisotropy is negative are given in Figure 14 and are showing once more that the spins are forced to be perpendicular to the $z$ axis, which in turn contrasts the bipolar boundary conditions.

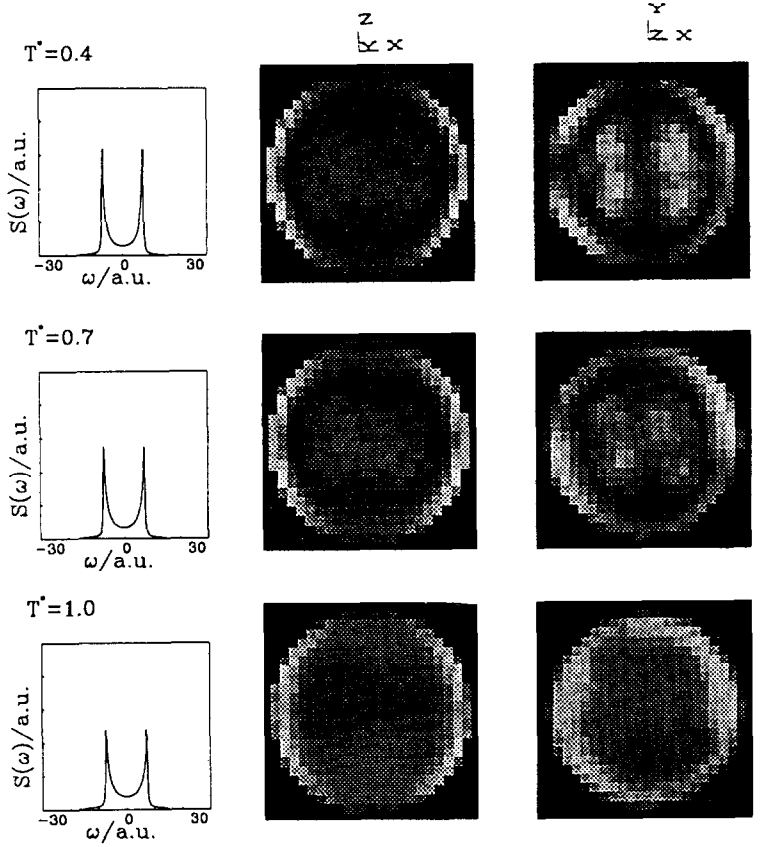


FIGURE 14. Same as Figure 12 for a negative applied field, $\xi = -0.5$.

## CONCLUSIONS

We have shown, starting from a purely microscopic interaction, that the thermodynamics of PDLC lattice models can be studied in great details by Monte Carlo simulations. Moreover we have determined the molecular organization and the ordering inside the droplet, and we have evaluated the dependence on the system size. We have presented results for homeotropic (radial boundary conditions) and planar (toroidal and bipolar boundary conditions) surface alignements. We have shown that the Monte Carlo method is a powerful tool to understand experimental data or even to predict results of new experiments. In fact from the simulated configurations, although the model employed is very simple, we have obtained static deuterium NMR lineshapes and polarized light microscopy textures that are in qualitatively agreement with experimental results when these are available. Our methods could also be useful in investigating the characteristics of surface alignment in PDLC in a situation where this is unknown. For instance, performing polarized light microscopy experiments the results could be compared to predicted simulation textures to help determining the kind of boundary conditions in the real system.

## ACKNOWLEDGEMENTS

We are grateful to MURST and CNR for support in particular through P.F. "Sistemi Informatici e Calcolo Parallelo" S.P.1. E.B. thanks the Swedish NFR and EEC HCM.

## REFERENCES

1. G.P. Crawford and J.W. Doane, Condens. Matter News, 1, 5 (1992).
2. J.W. Doane, MRS Bull., XVI, 22 (1991).
3. A. Golemme, S. Žumer, J.W. Doane, and M.E. Neubert, Phys. Rev. A, 37, 559 (1988).
4. S. Kralj and S. Žumer, Phys. Rev. A, 45, 2461 (1992).
5. N.D. Mermin, Rev. Mod. Phys., 51, 591 (1976).
6. J.H. Erdmann, S. Žumer and J.W.Doane, Phys. Rev. Lett., 64, 1907 (1990).
7. R. Ondris-Crawford, E.P. Boyko, B.G. Wagner, J.H. Erdmann, S. Žumer and J.W. Doane, J. Appl. Phys., 69, 6380 ( 1991).
8. R.D. Williams, J. Phys. A: Math. Gen., 19, 3211 (1986).
9. P. Drzaic, Mol. Cryst. Liq. Cryst., 154, 289 (1988).
10. R. Aloe, G. Chidichimo, and A. Golemme, Mol. Cryst. Liq. Cryst., 203, 1155 (1991).
11. J.W. Doane, N.A. Vaz, B.-G. Wu, and S. Žumer, Appl. Phys. Lett., 48, 269 (1986).
12. F. Xu, H.-S. Kitzerow and P.P. Crooker, Phys. Rev. A, 46, 6535 (1992).
13. S. Žumer, M. Vilfan, and I. Vilfan, Liq. Cryst., 3, 947 (1988).
14. N. Schopohl and T.J. Sluckin, J. Phys., 49, 1097 (1988).

15. C. Chiccoli, P. Pasini, F. Semeria, and C. Zannoni, Phys. Lett. A, 150, 311 (1990).
16. C. Chiccoli, P. Pasini, F. Semeria, and C. Zannoni, Mol. Cryst. Liq. Cryst., 221, 19 (1992).
17. E. Berggren, C. Zannoni, C. Chiccoli, P. Pasini, and F. Semeria, Chem. Phys. Lett., 197, 224 (1992).
18. C. Chiccoli, P. Pasini, F. Semeria, and C. Zannoni, Mol. Cryst. Liq. Cryst., 212, 197 ( 1992).
19. E. Berggren, C. Zannoni, C. Chiccoli, P. Pasini, and F. Semeria, Phys. Rev. E, 49, 614 (1994).
20. E. Berggren, C. Zannoni, C. Chiccoli, P. Pasini, and F. Semeria, submitted to Phys. Rev. E.
21. P.A. Lebwohl and G. Lasher, Phys. Rev. A, 6, 426 (1972).
22. U. Fabbri and C. Zannoni, Mol. Phys., 58, 763 (1986).
23. R. Berardi, A. Emerson, and C. Zannoni, J. Chem. Soc. Faraday Trans., 89, 4069 (1993).
24. D.G. Cleaver and M.P. Allen, Phys. Rev. A, 43, 1918 (1991).
25. Z. Zhang, O.G. Mouritsen and M. Zuckermann, Phys. Rev. Lett., 69, 2803 (1992).
26. G.R. Luckhurst and C. Zannoni, Nature, 267, 412 (1977).
27. G.R. Luckhurst, P. Simpson, and C. Zannoni, Chem. Phys. Lett. 78, 429 (1981).
28. G.S. Iannacchione, G.P. Crawford, J.W. Doane and D. Finotello, Mol. Cryst. Liq. Cryst., 222, 205 (1992).
29. C. Zannoni, J. Chem. Phys., 84, 424 (1985).
30. C. Chiccoli, P.Pasini, F. Semeria, T.J. Sluckin, C. Zannoni (to be published).
31. J.A. Schellman, in Polarized Spectroscopy of Ordered Systems, edited by B. Samori' and E.W. Thulstrup (Kluwer, 1988), p. 231.
32. A. Kilian, Liq. Cryst., 14, 1189 (1993).